

LASER MEDICINE

https://doi.org/10.1070/QEL16505

Effect of laser intensity and exposure time on photothermal therapy with nanoparticles heated by a 793-nm diode laser and tissue optical clearing

M. Aliannezhadi, M. Minbashi, V.V. Tuchin

Abstract. **Laser-induced thermotherapy is a promising method for cancer treatment, the outcome of which is affected by the exposure time. An inappropriate exposure time and laser intensity cause incomplete tumour destruction, tumour regrowth, and metastasis. Also possible is irreversible damage, i.e. death of healthy cells, and so numerical models are necessary to provide an optimised laser intensity and exposure time for different cancerous tumours. In this study, a model based on finite element method (FEM) is used for solving the bio-heat transfer equation and the Arrhenius equation describing tissue damage. The cancerous tumour is considered as a perfect cylinder with a diameter of 20 mm and a thickness of 2, 3, 4, and 5 mm, filled up by highly absorbing nanoparticles and surrounded by healthy cylindrical tissue with a diameter of 40 mm and a length of 10 mm, which ahs a low scattering coefficient due to optical clearing. The results show that 243 s is a safe and appropriate exposure time when a diode laser with a wavelength of 793 nm and intensity of 0.75 W cm^{-2} together with gold nanorods of concentration 0.0001% is used for the treatment of a 3-mm-thick tumour. Then, the results are developed and extensive numerical simulations are used to reveal mathematical relationships between two critical parameters, input power and optimised exposure time, for a series of different tumour thicknesses. Treatment protocols are presented.**

Keywords: *thermotherapy, nanoparticles, tissue optical clearing, cell death, cancerous tumor, bio-heat transfer equation, Arrhenius damage equation.*

1. Introduction

Cancer is a major cause of mortality worldwide [1]. Skin, breast, prostate and brain cancers are amongst the most common cancer types. A cancerous tumour is a result of abnormal proliferation of cells that divide and grow uncontrollably. They invade normal tissues and spread through the human body in the form of metastasis. For example, gliomas damaging brain and central nervous system are characterised by the ability to rapid proliferation, angiogenesis, and invasive growth [1–3]. From the standpoint of tissue optics, the differences between cancerous and surrounding normal tissues are more or less identical for various cancer types because rapid and thus irregular proliferation and invasive growth lead to an increase in the scattering coefficient, whereas tumour abnormal angiogenesis causes an increase in the absorption coefficient [4].

Many therapeutic methods such as chemotherapy, radiation therapy, hormone therapy, surgery and cryosurgery have been developed to treat different kinds of cancerous tumours [5]. Unfortunately, most modalities are not effective for treating metastasis. Also, they have severe side effects. For example, chemotherapy, i.e. a tumour treatment by using drugs, intravenous injections or oral medication, kills not only dividing, cancerous cells but also healthy cells. It reduces white blood cells and production of red blood cells by bone marrow. Immune suppression can be another negative result. In radiation therapy, ionising radiations such as X-rays, gamma rays, and particles like protons, neutrons, alpha particles are used in the treatment of different types of cancers such as melanomas. Radiation therapy has severe side effects such as skin burn, cavity in teeth, memory loss, vomiting, immune suppression, and loss of fertility [6].

Hyperthermia by some sources like laser, microwave, radiofrequency, and high-intensity focused ultrasound (HIFU) is used to heat and destroy a cancerous tumour [7–12]. In the case of skin cancerous tumour, using laser light is a promising method for the treatment whereas other ones have some disadvantages. For example, in the case of hyperthermia by radiotherapy, irregularities of the irradiated surface cause a nonuniform distribution of the administered dose, and the cancer tumour may regrow [13].

In 1963, Goldman et al. [14] reported the first research about the use of laser on the skin for dermatology. After that, an increasing number of activities have been investigated by using different lasers such as Nd:YAG [13] and CO_2 lasers [15]. The results show this method is effective, bloodless, and sterile. Heat control and prevention of its excessive rise in the tumour and normal tissue is one of the most important challenges in this area because an uncontrolled treatment can irreversibly damage patients' healthy tissue. To this end, many researchers are focused on theoretical and experimental studies using phantoms and laboratory animals in this field, including tumour heating by uploaded nanoparticles selectively and strongly absorbing laser radiation [8, 9, 12, 16–30]. Also, the dependence of the treatment efficiency on blood vessel discreteness and reactivity was considered [31, 32].

Some principal factors including laser intensity and wavelength, cancerous tumour and surrounding normal tissue

M. Aliannezhadi, M. Minbashi Physics Department, Semnan University, Semnan, Iran; e-mail: m_aliannezhadi@semnan.ac.ir;
V.V. Tuchin Education and Research Institute of Optics and Biophotonics, N.G. Chernyshevsky Saratov State University, ul. Astrakhanskaya 83, 410012 Saratov, Russia; Institute of Precision Mechanics and Control, Russian Academy of Sciences, ul. Rabochaya 24, 410028 Saratov, Russia; National Research Tomsk State University, prosp. Lenina 36, 634050 Tomsk, Russia;
e-mail: tuchinvv@mail.ru

Received 29 August 2017; revision received 21 January 2018
Kvantovaya Elektronika **48** (6) 559–564 (2018)
Submitted in English

type, as well as laser exposure time can affect laser thermotherapy outcomes. The laser wavelength is selected according to the absorption spectrum of different types of tissue and tumour, and determined the efficiency of tumour labelling by nanoparticles [27] and surrounding healthy tissue optical clearing [33, 34]. Also, choosing an inappropriate value of laser intensity and exposure time can progress the treatment in reverse. The necessity of accurate cancer treatment to destroy cancerous tumour completely with the least damage to healthy tissues requires some numerical simulations or experimental works. Numerical simulations can estimate the optimum conditions for all types and sizes of tumours in any region of the body to minimise the damage to the patient.

In this paper, a numerical approach is used to evaluate the cancerous tumour treatment by laser-induced thermal therapy. The aim of the current study is to find optimum exposure times for different laser intensities and tumour sizes for tumours uploaded by strongly absorbing nanoparticles and optically cleared surrounding healthy tissue [35, 36], which to the best our knowledge has not been previously reported. Through extensive numerical simulations, we reveal the mathematical relationships between two critical parameters in the photothermal therapy, input power and optimised exposure time for different tumour sizes.

2. Materials and methods

The incident laser light interacts with the cancer tumour and normal tissue. Then the light is scattered and absorbed by them [37, 38]. Thermal behaviour in the tissue can be described by using a bio-heat transfer equation, also known as Pennes equation, [37–40]:

$$\rho C\frac{\partial T}{\partial t}+\nabla(-k\nabla T)=\rho_{\mathrm{b}}C_{\mathrm{b}}\omega_{\mathrm{b}}(T_{\mathrm{b}}-T)+Q_{\mathrm{met}}+Q_{\mathrm{ext}}, \quad (1)$$

where ρ and ρ_{b} are the tissue and blood density (kg m^{-3}); C and C_{b} are the tissue and blood specific heat (J kg^{-1} K^{-1}); k is the tissue thermal conductivity (W K^{-1}); ω_{b} is the blood perfusion rate (s^{-1}); T and T_{b} are the temperature field and blood temperature (K); and Q_{met} and Q_{ext} are the heat source from metabolism and an external heat source generated by laser light absorption (W m^{-3}).

The absorption coefficient of tissue is low for light in the near-infrared wavelength range far from water absorption bands and therefor resonant nanoparticles or photosensitive agents are used to increase absorption, in particular to distinguish tumour cells by their labelling [41–46]. In the cylindrical coordinate, the external heat source created by laser absorption in the tumour is determined as follows:

$$Q_{\mathrm{las}}=-\frac{\partial I(r,z)}{\partial z}, \quad (2)$$

$$I(z)=I_0\exp[-(\mu_{\mathrm{a}}+\mu_{\mathrm{s}})z], \quad (3)$$

where the Beer–Lambert law is used for laser light distribution. The law is used when $\mu_{\mathrm{s}}=N\sigma_{\mathrm{sca}}\ll 1/L$, where N, σ_{sca} and L are the number density of scatterers, the scattering cross-section and the thickness of the media, respectively [27, 28]; I_0 is the laser intensity (W cm^{-2}); and r and z are the spatial cylindrical coordinates. The absorption μ_{a} (cm^{-1}) and scattering μ_{s} (cm^{-1}) coefficients are determined from the formulas [29]:

$$\mu_{\mathrm{a}}=\mu_{\mathrm{am}}+\mu_{\mathrm{an}}, \quad (4)$$

$$\mu_{\mathrm{s}}=\mu_{\mathrm{sm}}+\mu_{\mathrm{sn}}, \quad (5)$$

where μ_{am} and μ_{an} are the absorption of the human tissue and nanoparticles, respectively; and μ_{sm} and μ_{sn} are the scattering coefficients of the human tissue and nanoparticles, respectively. The quantities μ_{an} and μ_{sn} can be calculated as follow [30]:

$$\mu_{\mathrm{an}}=0.75f_v\frac{Q_{\mathrm{a}}}{r_{\mathrm{eff}}}, \quad (6)$$

$$\mu_{\mathrm{sn}}=0.75f_v\frac{Q_s}{r_{\mathrm{eff}}}, \quad (7)$$

where f_v and r_{eff} are the volume fraction and the effective radius of nanoparticles; and Q_{a} and Q_{s} are the dimensionless efficiency factor of absorption and scattering for a single particle.

The thermal damage induced in the tumour and tissue was estimated as a function of temperature, an energy barrier, and time by using the Arrhenius model. The dimensionless damage parameter α characterises the rate of injury k_{d}, which is given by the equation [41–47]:

$$k_{\mathrm{d}}=\frac{\mathrm{d}\alpha}{\mathrm{d}t}=A\exp\left(\frac{-E_{\mathrm{a}}}{RT(t)}\right), \quad (8)$$

where A is the frequency factor (s^{-1}); E_{a} is the 'activation' energy barrier for irreversible damage reaction (J mol^{-1}); R = 8.3143 J mol^{-1} K^{-1} is the universal gas constant; and $T(t)$ is the absolute temperature as a function of time t. The value of $\alpha=1$ is a threshold value for estimating the extent of the ablation zone, and A and E_{a} are dependent on the type of tissue. The volume fraction of necrotic tissue, θ_{d}, is then expressed as [46, 47]

$$\theta_{\mathrm{d}}=1-\exp(-\alpha). \quad (9)$$

In the first step, tumour is considered as a cylindrical cancerous tumour with a diameter of 20 mm and a thickness of 3 mm. Then, the developed model is applied to other tumour thicknesses. The tumour is surrounded by cylindrical healthy tissue. The geometry of laser/tumour and normal tissue models in the first study is shown in Fig. 1. As shown in Fig. 1, the boundary conditions for the first study are as follows: The upper boundary at z = 10 mm is subjected to convective, radiative heat flux boundary conditions before and after transient cooling. The bottom boundary and boundary at r = 20 mm are normally at the core body temperature, so temperature in the boundaries is constant for all times and $T_{\mathrm{r}}=T_{\mathrm{b}}$, where T_{b} is the patient's body temperature.

Gold nanorods (GNRs) with an aspect ratio of 3.9 and effective radius of 11.43 nm are adopted to obtain a high absorption efficiency. The plasmon maximum of the nanorod suspension lies in the near-IR region around 800 nm; therefore, we used a diode laser with a wavelength of 793 nm and equations (4)–(7) to calculate the scattering and absorption coefficients at this wavelength. According Refs [48, 49], these equations satisfactorily describe real tissues. One of the most flexible and powerful methods for computing the optical properties of particles with an arbitrary geometry – the discrete dipole approximation (DDA) – was used to calculate the optical properties of nanorods. The nanorod was considered

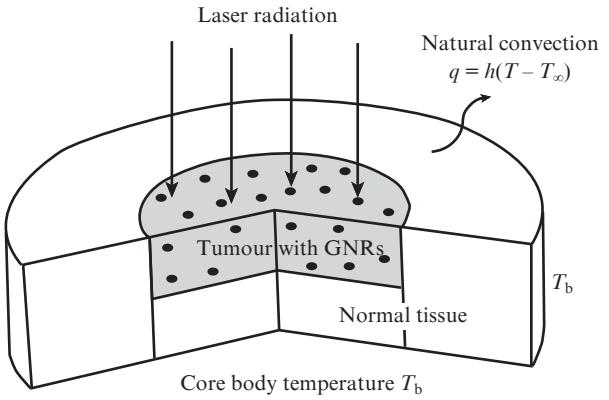

Figure 1. Geometry of the interaction model of a laser beam with healthy tissue of diameter 40 mm and tumour of diameter 20 mm and thickness 3 mm witt GNRs. Healthy and tumour tissues are optically cleared (see Table 1), i.e. have a low scattering coefficient allowing for use of Eqn. (3) to calculate laser beam attenuation in tissue.

as a cylinder capped with two hemispheres. To specify the size and volume V of a cylindrical nanorod, an effective radius r_{eff}, equal to the radius of a sphere of the same volume V:

$$r_{eff} = (3V/4\pi)^{1/3}. \quad (10)$$

Thermal and optical parameters for healthy surrounding and tumour tissues with GNRs, which were used in the simulation, are summarised in Table 1. It also lists the blood specific heat (4200 J kg^{-1} K^{-1}) [50] and optical properties for tissues and nanoparticle suspension, which correspond to the wavelength of a diode laser used for the modelling, i.e., 793 nm. Due to specificity of optical clearing technology [35], for tumours it is more efficient to provide intratumoral injection, which can be done together with nanoparticles as their suspension in glycerol, glucose, polyethylene glycol (PEG) or Iohexol (Omnipaque^{TM}), a non-ionic, water-soluble radiographic contrast agent with iodine [24, 25, 51–53]. We can suppose that for such injection in a definite time after injection nanoparticles will be distributed within tumour and, thus, the absorption coefficient will be much higher than before (121 cm^{-1} instead of 0.02 cm^{-1}), the scattering coefficient will be significantly reduced to 0.5 cm^{-1} due to the refractive index matching effect, and due to diffusivity of an optical clearing agent into surrounding tissue, its scattering coefficient will be also reduced but to a lesser value of 6.5 cm^{-1} instead of its typical value of 100–200 cm^{-1} for a wavelength of 793 nm [4].

The thermal distribution and thermal damage are estimated by solving the bio-heat transfer equation and the thermal damage function simultaneously. The finite element method (FEM) is a useful numerical technique for the thermal process [8, 12, 17, 18, 46–47, 50, 54–58]. Thus, Eqns (1)–(9) are solved numerically using the FEM method by COMSOL Multiphysics® software (Heat Transfer module) (COMSOL, Inc., Burlington MA, USA) to find the optimum conditions in the treatment. The numerical simulation of laser photothermal therapy is done in the paper to find optimum conditions for cancerous tumour treatment. The simulation was based on the FEM model.

3. Results and discussion

First, the results are compared with those from Ref. [27] for validation. The schematic of the model is shown in Fig. 2a. The geometry dimensions are set as in Ref. [27], and a laser exposure of 150 s, laser intensity of 0.5 W cm^{-2}, and GNR volume fraction of 0.001% are used for simulation. Temperature contours of 40, 50 and 60 °C are plotted in Fig. 2b. For comparison, the results of Ref. [27] are presented in the figure. The results indicate that they perfectly match together and so our simulation is valid.

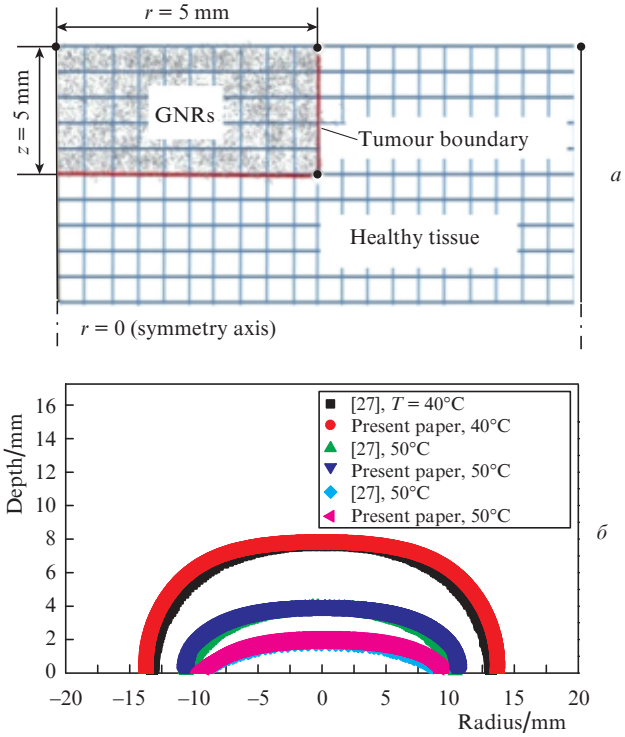

Figure 2. (Colour online) (a) Schematic of the structure and boundaries from Ref. [27] and (b) comparison of our result with temperature contours of 40, 50 and 60 °C with those of Ref. [27].

After validation, we use our structure, boundary condition in Fig. 1, and 0.0001% GNR volume fraction to perform the simulations. The temperature distribution in the cancerous tumour and normal tissue are shown in Fig. 3 for two different intensities and laser exposure times of 50 and 500 s.

Table 1. Thermal parameters of healthy tissue and tumour with GNRs used in the simulation.

Type of layer	ρ/kg m^{-3}	k/W mK^{-1}	ω_b/s^{-1}	C_b/J kg^{-1} K^{-1}	μ_a/cm^{-1}	μ_s/cm^{-1}	A/s^{-1}	E_a/mJ mol^{-1}
Normal tissue (partly optically cleared)	1000 [50]	0.5 [50]	1×10^{-3} [50]	4200 [50]	0.02 [50]	6.5 [4, 27, 50]	5.24×10^{91} [58]	6.28×10^{5} [58]
Optically cleared tumour tissue with 0.001%	1100 [50]	0.55 [50]	9.1×10^{-4} [50]	4200 [50]	121 [27, 50]	0.5 [4, 27, 50]	5.24×10^{91} [58]	6.28×10^{5} [58]

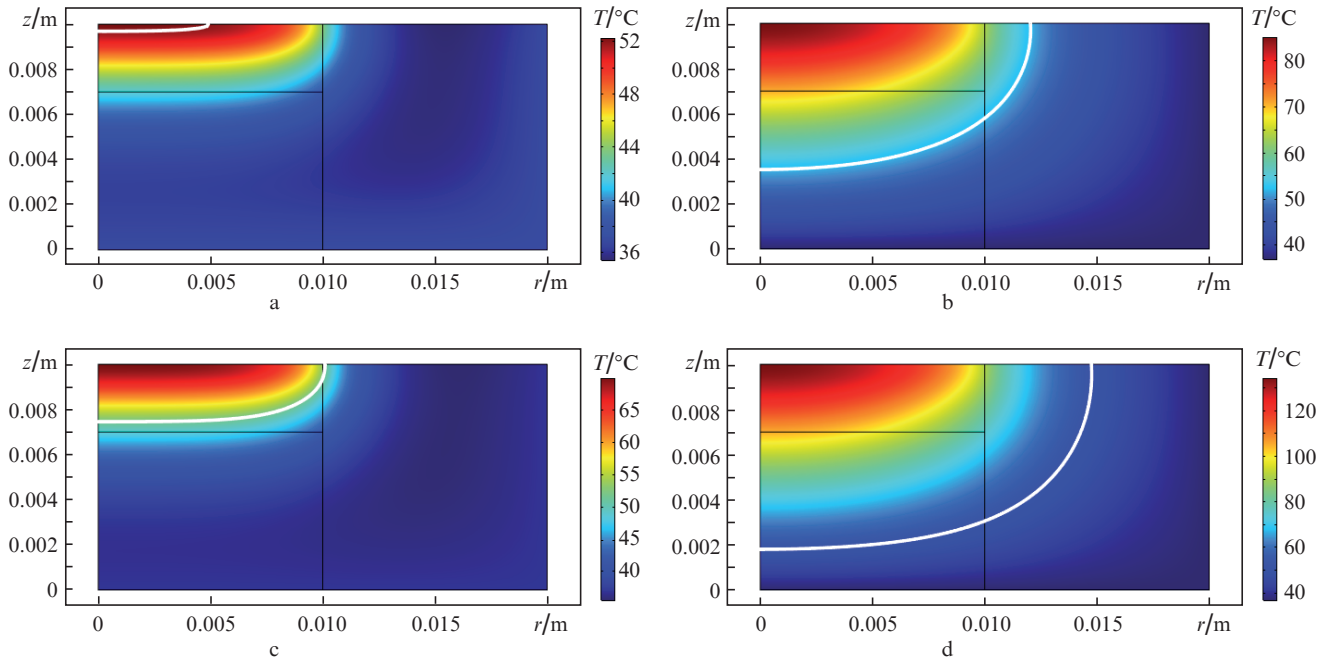

Figure 3. (Colour online) Temperature distributions in tumour and normal tissue for (a) $I = 0.5$ W cm^{-2} and exposure times $t = 50$ s; (b) $I = 0.5$ W cm^{-2}, $t = 500$ s; (c) $I = 1$ W cm^{-2}, $t = 50$ s; (d) $I = 1$ W cm^{-2}, $t = 500$ s. The white lines are the temperature contours of 52 °C.

The results show that for each exposure time the maximum temperatures are in the centre of tumour and temperatures decrease towards the edge of the tumour. For example, at 0.5 W cm^{-2} and an exposure time of 50 s, the temperatures in the centre and at the edge of tumour are 52.3 °C and 38.6 °C, respectively. Also, the overall temperatures rise with increasing exposure time. Comparison of results in Figs 3a and 3c or Figs 3b and 3d shows that the laser intensity strongly affects the temperature of different regions during each exposure time. The temperature contours of 52 °C are shown as a white line in Fig.3.

Temporal behaviour of temperature at four position exposed by the central part of the laser beam with intensity $I = 0.5$ W cm^{-2} is shown in Fig. 4 to compare with our previous experimental results [21]. First, the temperature rises rapidly at all points, and then the slope decreases and finally temperature at each point reaches a constant value (each dependence saturates). These results are consistent with our experimental data [21].

Figure 5 shows the distribution of the fraction of necrotic tissue, θ_d, for a laser intensity of 0.5 W cm^{-2} and two different exposure times of 50 and 1000 s. One can see (Fig. 5a) that for an exposure time of 50 s a small part of tumour is destroyed and a significant portion of the tumour remains, and so if the irradiation process is stopped in this step, the tumour will

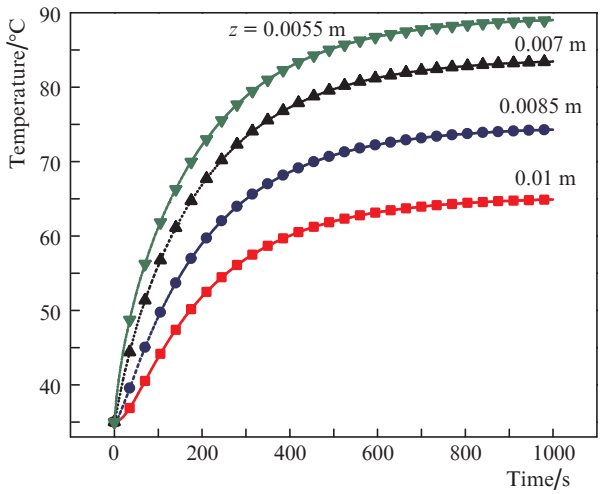

Figure 4. Temporal dependences of the temperature at four position of the tumour exposed to the central part of the laser beam with $I = 0.5$ W cm^{-2}. At $r = 0$ and different z.

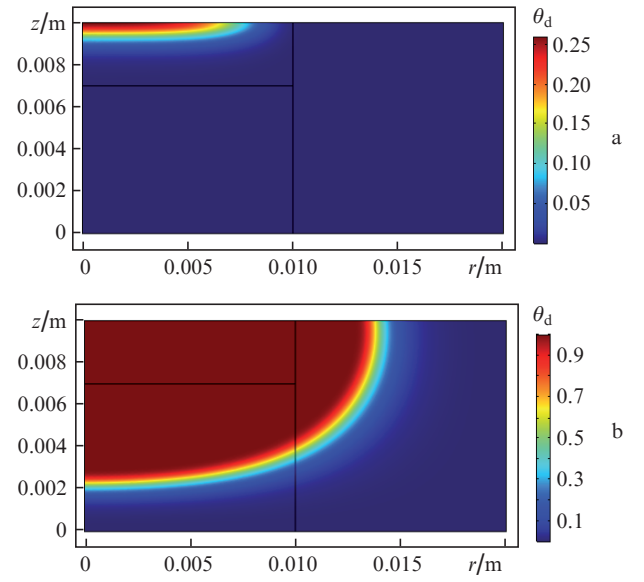

Figure 5. (Colour online) Fraction of necrotic tissue distribution, θ_d, in the tumour and normal tissue at a laser intensity of 0.5 W cm^{-2} and two exposure times of (a) 50 and (b) 1000 s.

regrow. Depending on the type of tumour, metastasis can lead to new cancerous tumours far from the first one and it can damage vital organs in the patient's body. Figure 5b shows an ellipse area with large and small diameters of 25 mm and 13.8 within which tumour is destroyed completely after an exposure time of 1000 s.

To find an optimum exposure time for successful therapy, Fig. 6 shows nine different positions and Fig. 7 demonstrates temporal developments of the fraction of necrotic tissue for an intensity of 0.75 W cm^{-2} at these points. According to the results, the fraction of necrotic tissue rapidly increases and reaches a maximum value for every tumour position. The fraction of necrotic tissue at the $r = 0$, $z = 0.01$ m and $r = 0.01$ m, $z = 0.007$ m increases rapidly at an average rate of 1.82×10^{-4} and 7.96×10^{-4} s^{-1} and reaches a unity at an exposure time of 48 s and 243 s, respectively; therefore, 243 s is an optimum time because cancer cells are destroyed completely and the healthy tissue suffer the least damage.

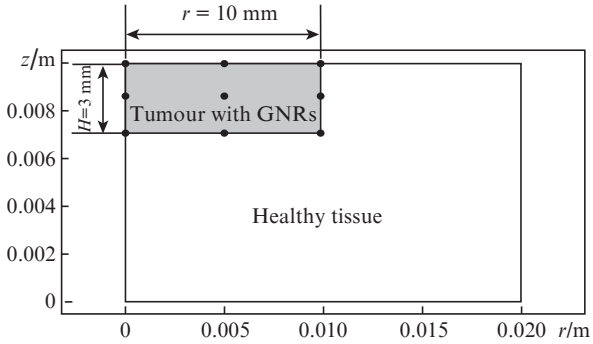

Figure 6. Nine different positions of the tumour in which the fraction of necrotic tissue was simulated as a function of time.

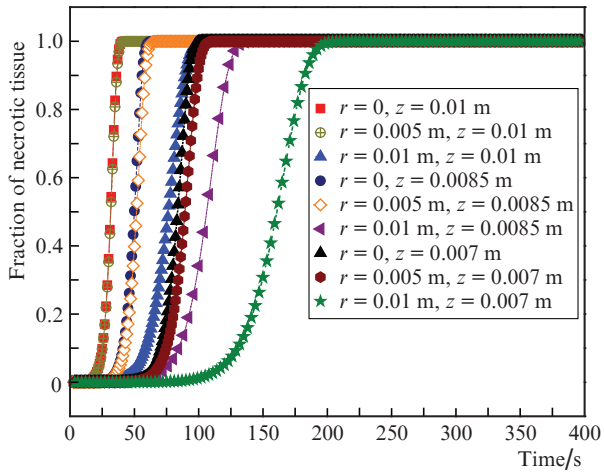

Figure 7. (Colour online) Temporal developments of the fraction of necrotic tissue at nine different positions shown in Fig. 6 at a laser intensity of 0.75 W cm^{-2}.

Thus, we have found an optimum exposure time for one special intensity level of 0.75 W cm^{-2}. In the next step, the model is developed and extensive numerical simulations are performed to find the optimum exposure time for every intensity level and a tumour thickness of 3 mm. Then, the results are extended to find optimum parameters for the different cancerous tumour thicknesses (H = 2, 3, and 4 mm). The treatment protocols are presented in Fig. 8 for the different cancerous tumour thicknesses (H = 2, 3, 4, and 5 mm) and various laser intensities. According to the results, for low laser intensity levels the optimum laser exposure times are more dependent on the tumour thickness than for the high one.

The optimum values in Fig. 8 reveal the mathematical relationships between two critical parameters for each of the four tumour thicknesses. These four categories of data can be accurately approximated by the function $t_{exp} = a + bc^I$. Also, the constants are collected in Table 2 for different categories. According the mathematical relationships, the optimum parameters and treatment protocol will be clear for different conditions.

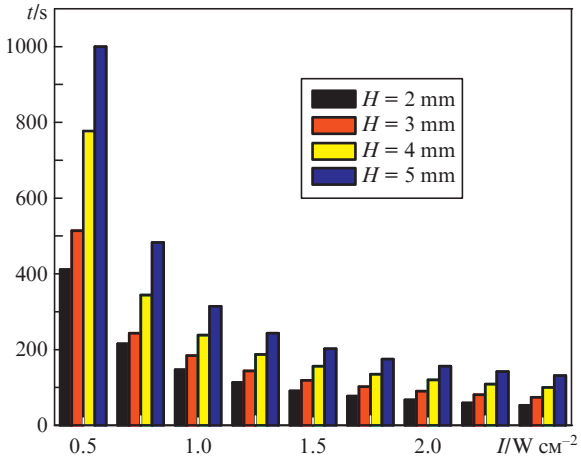

Figure 8. Treatment protocols for the different cancerous tumour thicknesses.

Table 2. Exponential constants for different cancerous tumour thicknesses.

H/mm	a	b	c
2	62.9	1453.9	0.0558
3	87.38	1952.8	0.0464
4	123.6	4333.1	0.02227
5	154.67	4665.1	0.03227

4. Conclusions

Any abnormal proliferation of cells and the body's inability to fix the problem lead to cancerous tumours. It can spread through the patient's body and disrupt the functioning of the body and cause serious health problems. Many therapeutic methods have severe side effects. Photothermal therapy mediated by plasmonic nanoparticles is a promising method in cancer therapy. In the paper, thermotherapy with laser-induced heating of embedded plasmonic nanoparticles is considered for cancerous tumour treatment at optical clearing of surrounding healthy tissue. In the first step, a diode laser with a wavelength of 793 nm and an intensity of 0.5 W cm^{-2} is used for simulations and then it is developed to other intensities. Also, the tumour is considered as a cylindrical cancerous tumour with a diameter of 20 mm and a thickness of 3mm, and then other thicknesses are studied too. A two-dimensional model based on the finite element method is used for solving the bio-heat transfer equation and the Arrhenius

damage model is used to evaluate the fraction of necrotic tumour tissue at laser ablation. The treatment outcome is dependent on the laser intensity and exposure time; through extensive numerical simulations the mathematical relationships are revealed between them and treatment protocols are presented for four different tumour thicknesses (H = 2, 3, 4, and 5 mm). The result obtained is appropriate for many different soft tissue types, including brain, prostate, breast, due to tumour labelling by nanoparticles and reduction of the scattering coefficient of tissues under study. Both procedures eliminate inherent scattering and absorption properties and make them universal and controllable, by ensuring high tumour absorption and low tumour and surrounding tissue scattering.

Acknowledgements. The work of V.V.T. was supported by the Ministry of Education and Science of the Russian Federation (Grant No. 17.1223.2017/AP) and the Russian Foundation for Basic Research [Grant Nos 17-02-00358 and 17-00-00272 (17-00-00275 (K))].

References

1. http://www.medicalnewstoday.com/info/cancer-oncology.
2. Raizer J., Parsa A. (Eds.) *Current Understanding and Treatment of Gliomas* (Switzerland: Springer International Publishing, 2015).
3. Zavadskaya T.S. *Exp. Oncol*., **37** (4), 234 (2015).
4. Tuchin V.V. *Tissue Optics: Light Scattering Methods and Instruments for Medical Diagnosis* (Washington: SPIE Press, 2015).
5. https://www.cancer.gov/about-cancer.
6. Sudhakar A. *Cancer Sci. Ther*., **1** (2), 1 (2009).
7. Lepock J.R. *Int. J. Hyperthermia*, **19** (3), 252 (2003).
8. Alisoy H.Z., Us B.S., et al. *Optik*, **124** (21), 5218 (2013).
9. Wang T., Zhao G., et al. *Int. J. Heat Mass Transfer*, **90**, 81 (2015).
10. Poon S., Cooper R., et al. *Int. J. Card.*, **222**, 772 (2016).
11. Johnson S., Dillon C., et al. *Int. J. Hyperthermia*, **32** (7), 723 (2016).
12. Mi Y., Rui S., et al. *Med. Biol. Eng. Comput*., **55** (7), 1109 (2017).
13. Moskalik K., Kozlov A., et al. *Photomed. Laser Surg*., **27** (2), 345 (2009).
14. Goldman L., Blaney D., et al. *Nature*, **197**, 912 (1963).
15. Hibler B.P., Sierra H., et al. *Br. J. Dermatol*., **174** (6), 1359 (2016).
16. Mochnacki B., Majchrzak E. *Int. J. Heat Mass Transfer*, **108**, 1 (2017).
17. Vyas C.M.D., Kumar S. *Int. J. Heat Mass Transfer*, **99**, 122 (2016).
18. Sánchez S., Bautista O., et al. *Int. J. Heat Mass Transfer*, **90**, 728 (2015).
19. Bhowmik A., Repaka R. *Int. J. Heat Mass Transfer*, **98**, 81 (2016).
20. Kumar S., Srivastava A. *Int. J. Heat Mass Transfer*, **90**, 466 (2015).
21. Terentyuk G.S., Maslyakova G.N., et al. *J. Biomed. Opt*., **14** (2), 021016-1-8 (2009).
22. Feng Y., Fuentes D., et al. *Eng. Comput.*, **25** (1), 3 (2009).
23. Mackey M.A., Ali M.R.K., et al. *J. Phys. Chem. B*, **118** (5), 1319 (2014).
24. Bucharskaya A., Maslyakova G., et al. *Int. J. Mol. Sci*., **17** (8), 1295 (2016).
25. Bucharskaya A.B., Maslyakova G.N., et al. *BioNanoSci*., **7** (1), 216 (2017).
26. Yakunin A.N., Avetisyan Y.A., et al. *J. Biomed. Opt*., **20** (5), 051030 (2015).
27. Soni S., Tyagi H., et al. *J. Therm. Biol.*, **43**, 70 (2014).
28. Gaponenko S.V. *Introduction to Nanophotonics* (Cambridge: Cambridge Univ. Press, 2010).
29. Vera J., Bayazitoglu Y. *Int. J. Heat Mass Transfer*, **52** (3), 564 (2009).
30. Dombrovsky L.A., Timchenko V., et al. *Int. J. Heat Mass Transfer*, **54** (25), 5459 (2011).
31. Lubashevsky I.A., Priezzhev A.V. *J. Biomed. Opt*., **4** (2), 248 (1999).
32. Datsko B.Y., Gafiychuk V.V., et al. *J. Med. Eng. Technol.*, **30** (6), 390 (2006).
33. Genina E.A., Bashkatov A.N., et al. *Expert Rev. Med. Devices*., **7** (6), 825 (2010).
34. Genina E.A., Bashkatov A.N., et al. *J. Biomed. Photon. Eng*., **1** (1), 22 (2015).
35. Tuchin V.V. *Optical Clearing of Tissues Blood* (Bellingham, WA: SPIE Press, 2006).
36. Lee S., Bindokas V., et al. *Sci. Rep*., **7** (1), 1 (2017).
37. Niemz M.H. *Laser-Tissue Interactions: Fundamentals Applications* (Berlin, Heidelberg, New York: Springer, 2007).
38. Welch A.J., van Gemert M.J.C. *Optical-Thermal Response of Laser-Irradiated Tissue* (Berlin, Heidelberg, New York: Springer Sci. + Business Media, 2011).
39. Pennes H. *J. Appl. Physiol.*, **1** (2), 93 (1948).
40. Wissler E. *J. Appl. Physiol*., **85** (1), 35 (1998).
41. Jacques S.L. *J. Biomed. Opt*., **11** (4), 041108-7 (2006).
42. Pearce J.A. *Proc. SPIE*.,**7181**, 718104-15 (2009).
43. Thomsen Sh., Pearce J.A., in *Optical-Thermal Response of Laser-Irradiated Tissue* (Berlin, Heidelberg, New York: Springer Sci. + Business Media, 2011) Ch. 13, p. 487.
44. Pearce J.A. *Int. J. Hyperthermia*, **29** (4), 262 (2013).
45. van Rhoon G.C. *Int. J. Hyperthermia*, **32** (1), 50 (2016).
46. Schutt D.J., Haemmerich D. *Med. Phys*., **35**, 3462 (2008).
47. He X., McGee S., Coad J.E., et al. *Int. J. Hyperthermia*, **20**, 567 (2004).
48. Jain P.K., Lee K.S., et al. *J. Phys. Chem. B*, **110** (14), 7238 (2006).
49. Kannadorai R., Liu Q. *Med. Phys. J*., **40** (10), 103301-11 (2013).
50. Ren Y., Qi H., et al. *Int. J. Heat Mass Transfer*, **106**, 212 (2016).
51. Genina E.A., Bashkatov A.N., et al. *J. Biomed. Photon. Eng.*, **1** (1), 22 (2015).
52. Sdobnov A., Darvin M.E., et al. *J. Biophoton*., **10** (9), 1115 (2017).
53. Sdobnov A.Yu., Tuchin V.V., et al. *J. Phys. D: Appl. Phys.*, **50** (28), 1 (2017).
54. Chen G., Gu X., et al. *Optik*, **127**, 10115 (2016).
55. Chen G., Bi. J. *Optik*, **131**, 574 (2017).
56. Xu F., Lu T.J. *Introduction to Skin Biothermomechanics Thermal Pain* (Berlin, Heidelberg: Springer-Verlag, 2011).
57. Jesús Cepeda Rubio M.F. *Nanomed. J*., **3**, 2 (2011).
58. Xu F., Seffen K., Lu T. *IAENG Int. J. Comput. Sci*., **35** (1), 92 (2008).